

Lawrence Berkeley National Laboratory

Lawrence Berkeley National Laboratory

Title

Titanate Anodes for Sodium Ion Batteries

Permalink

<https://escholarship.org/uc/item/5cc8g1d4>

Author

Doeff, Marca

Publication Date

2014-01-31

Peer reviewed

This document was prepared as an account of work sponsored by the United States Government. While this document is believed to contain correct information, neither the United States Government nor any agency thereof, nor the Regents of the University of California, nor any of their employees, makes any warranty, express or implied, or assumes any legal responsibility for the accuracy, completeness, or usefulness of any information, apparatus, product, or process disclosed, or represents that its use would not infringe privately owned rights. Reference herein to any specific commercial product, process, or service by its trade name, trademark, manufacturer, or otherwise, does not necessarily constitute or imply its endorsement, recommendation, or favoring by the United States Government or any agency thereof, or the Regents of the University of California. The views and opinions of authors expressed herein do not necessarily state or reflect those of the United States Government or any agency thereof or the Regents of the University of California.

Titanate Anodes for Sodium Ion Batteries

Marca M. Doeff^{*}, Jordi Cabana,[§] and Mona Shirpour

Environmental Energy Technologies Division

Lawrence Berkeley National Laboratory

University of California

Berkeley, CA 94720

^{*}Corresponding author: mmdoeff@lbl.gov, tel: (510) 486-5821

[§] current address: Department of Chemistry, University of Illinois at Chicago

845 W. Taylor Street, Science & Engineering South (MC 111) Chicago, IL 60607

Acknowledgment

This work was supported by the Laboratory Directed Research and Development Program of Lawrence Berkeley National Laboratory under U.S. Department of Energy Contract DE-AC02-05CH11231.

Abstract

For reasons of cost and supply security issues, there is growing interest in the development of rechargeable sodium ion batteries, particularly for large-scale grid storage applications. Like the much better known and technologically important lithium ion analogs, the devices operate by shuttling alkali metal cations between two host materials, which undergo insertion processes at different electrochemical potentials. In the case of the lithium systems, there are several choices of host materials, but the most common positive electrode (cathode) material is the layered oxide, LiCoO_2 , and the most widespread negative electrode (anode) in use is graphite. Although there are also several options for cathode materials for the corresponding sodium systems, a significant impediment to their development is the lack of a suitable anode material, due to the fact that sodium does not intercalate into graphite. Researchers have investigated alternatives, such as hard carbons and alloys with tin or other metals, but all suffer from drawbacks such as poor safety characteristics or large volume changes that negatively impact the cycling behavior. The most promising options at present lie with titanates, not in the least because of attractive characteristics such as low toxicity, ease of synthesis, wide availability, and low cost. Of particular interest are sodium titanates, some of which insert sodium at unusually low potentials with high gravimetric capacities, and show good cycling behavior.

Keywords: sodium ion battery, anodes, titanates, sodium nonatitanate, lepidocrocite structures

Introduction

The commercialization of lithium ion batteries, which began in 1991, has enabled the recent revolution in portable electronics. As of 2010, the worldwide market was approximately \$US 11 billion and it is projected to grow to over \$US 40 billion by 2020, as hybrid electric vehicles (HEVs), plug-in hybrids (PHEVs) and all electric vehicles (EVs) are increasingly produced and adopted [1]. The need for large battery packs for these vehicles is expected to put pressure on lithium supplies [2] and drive up costs in the short term. This trend is further exacerbated if these batteries are also used for large-scale grid storage, as is presently being considered [3]. For these reasons, interest in alternative energy storage devices, particularly for the latter application, has never been higher than the present. Because of the wide availability and low cost of sodium-containing precursors, one extremely attractive possibility is the sodium ion battery [4, 5]. Like the more familiar Li ion counterpart, it is a dual intercalation system, in which both positive and negative electrodes undergo reversible electrochemical alkali metal ion insertion processes. (The shuttling of ions between the two electrodes as the cells charge and discharge inspired nicknames such as “rocking chair” or “shuttlecock” batteries in the early days of research). While batteries with lithium metal anodes have much higher theoretical energy densities than those with sodium, there is not necessarily an intrinsic energy density penalty when transitioning from a dual intercalation system based on lithium to one based on sodium, because energy density is determined by the potential differences and equivalent weights of the host structures used as electrodes, rather than

that of the alkali metals themselves. Thus, the key to successful development of sodium ion batteries lies with identifying materials with suitably high capacities for sodium insertion and appropriate potentials (high for cathode materials and low for anodes). Several attractive cathode materials have now been investigated for sodium ion systems; including the tunnel compound $\text{Na}_{0.44}\text{MnO}_2$ [6, 7, 8], layered transition metal oxides [9, 10] and polyanionic compounds [11]. There are fewer choices for anodes, in part, because sodium does not insert into graphite, the most commonly employed anode in lithium ion batteries. Instead, research efforts have been directed towards disordered carbons [12], which insert variable amounts of sodium ions, depending on details of the structure [13]. Reversible capacities as high as 250 mAh/g have been obtained [14] but concerns about the safety of the sodiated electrodes [15] may prohibit utilization in real devices. Some binary alloys of sodium with tin, lead or other metals are expected to have very high gravimetric capacities and low potentials, but the volumetric energy densities are much less than those found with lithium alloys, due to the larger size of sodium ions [16]. In addition, the enormous volume changes (often several hundred percent) associated with the alloying processes are expected to cause rapid degradation of the electrode, leading to poor cycling behavior, as is observed with some of the lithium alloy systems such as Li/Si. Conversion electrodes such as binary metal oxides, which are reduced completely to the element and the alkali metal oxide during discharge, have high capacities and fairly low potentials, but suffer from poor cycling behavior and low round trip efficiencies [17] due to the high degree of structural rearrangement that occurs.

The best possible alternative at this time is an intercalation compound that inserts sodium at low potentials, such as a titanate. Titanates are attractive because of their low

toxicity, wide abundance and low cost. Lithium insertion is known to occur at reasonably low voltages between about 1-2V vs. Li^+/Li for the binary structures. The shapes of the voltage profiles and the practical capacities obtained vary depending on the structure (anatase, rutile, brookite, etc.) and the extent of nanostructuring [18]. The most technologically important titanate for battery applications, however, is the spinel $\text{Li}_4\text{Ti}_5\text{O}_{12}$ [19]. Lithium ions in this structure cannot be extracted because that would require oxidation of Ti past +4, but reductive lithium insertion and subsequent oxidative lithium extraction occurs via a two-phase reaction mechanism ($\text{Li}_4\text{Ti}_5\text{O}_{12} + 3\text{Li}^+ + 3\text{e}^- \leftrightarrow \text{Li}_7\text{Ti}_4\text{O}_{12}$) at about 1.5V vs. Li/Li^+ . Because there is almost no change in volume between the two phases, the reaction is highly reversible. The relatively high voltage and modest theoretical capacity (170 mAh/g), however, restrict use as an anode material in lithium ion batteries to applications that do not require high energy density, such as HEVs.

The larger size of the sodium ion (1.02 Å) compared to the lithium ion (0.76 Å) [20] means that sodium insertion into the binary titanates is not expected to occur to an appreciable extent, even with extensive nanostructuring. One exception appears to be that of amorphous TiO_2 nanotubes having inner diameters greater than 80 nm [21], which have a reversible capacity of about 150 mAh/g between 2.6-1V vs. Na/Na^+ . Interestingly, sodium does insert into $\text{Li}_4\text{Ti}_5\text{O}_{12}$ at about 1V vs. Na/Na^+ with a capacity of 145 mAh/g [22, 23]. Based on the flat voltage profile, x-ray diffraction evidence, and advanced scanning transmission electron microscope imaging techniques, the redox reaction has been shown to take place by an unusual 3-phase mechanism; $\text{Li}_4\text{Ti}_5\text{O}_{12} + 3\text{Na}^+ + 3\text{e}^- \leftrightarrow \frac{1}{2} \text{LiNa}_6\text{Ti}_5\text{O}_{12} + \frac{1}{2} \text{Li}_7\text{Ti}_5\text{O}_{12}$. Unlike the case with lithium insertion, the electrochemical

reaction of $\text{Li}_4\text{Ti}_5\text{O}_{12}$ with larger sodium ions is unlikely to be a zero-strain process; thus, the long-term cyclability of this electrode still needs to be established. These two examples of titanates as sodium insertion hosts illustrate the utility of investigating this chemistry for battery applications. Further study is likely to identify phases with higher energy densities (lower potentials vs. Na/Na^+ and higher capacities), more attractive voltage characteristics, and improved reversibility. For example, ternary titanates, particularly those belonging to the Na-Ti-O system, have diverse structural and physical characteristics making them of particular interest for use in batteries, as well as other applications. Herein, we discuss the structural and electrochemical characteristics of several other titanates, focusing on the sodium intercalation processes.

Experimental

$\text{Na}_2\text{Ti}_6\text{O}_{13}$ was synthesized by a solid-state reaction using stoichiometric amounts of TiO_2 (anatase, purity 99.7%, <25 nm, Sigma-Aldrich) and Na_2CO_3 (purity 99.95+%, Aldrich). The mixture was calcined at 800°C for 20 h, followed by grinding, mixing, pelletizing, and a second calcination at 800°C for 20 h. $\text{NaTi}_3\text{O}_6(\text{OH})\cdot 2\text{H}_2\text{O}$, also known as sodium nonatitanate, was synthesized hydrothermally as previously described [24] Deionized water (5 mL) was first added to a 50 wt% NaOH solution (7.8 g, Sigma-Aldrich). Then titanium isopropoxide (6.25 g, purity 97%, Aldrich) was added rapidly to the solution while stirring. The white gel that formed in the beaker was mixed for about 10 min and then transferred to a pressure vessel with a 30 mL size Teflon lining, for treatment at 200°C for twenty hours. The product was filtered, washed and dried under vacuum at 120°C for 12 h. It was then subjected to a heat treatment at 600°C for two hours to make an anhydrous compound structurally related to the nonatitanate phase.

$K_{0.8}[Ti_{1.73}Li_{0.27}]O_4$ (KTL) was prepared via the solid-state reaction of Li_2CO_3 (purity 99.4%, Sigma), K_2CO_3 (purity 99.0%, Sigma-Aldrich), and TiO_2 (anatase, purity 99.7%, <25 nm, Sigma-Aldrich) at 800°C for 20 hours [25]. The protonated form of KTL (abbreviated as H-KTL) was prepared by leaching the starting material in a 1M aqueous solution of HCl (Solution/solid=100 cm³/g) at room temperature until all of the potassium was removed, as judged from X-ray diffraction experiments, energy dispersive x-ray spectroscopy (EDS) coupled with scanning electron microscopy (SEM) and Raman spectroscopy (see below). To produce the sodium form (abbreviated as Na-H-KTL), the protonated form was stirred in 1M NaOH (Solution/solid=100 cm³/g) at room temperature for 7 days in a closed vial. Then it was filtered, washed and dried at 110°C for 20 hours.

The phase purity of materials was determined by X-ray powder diffraction (XRD) using a Philips PW3040 X'Pert Pro diffractometer with a Cu K α ($\lambda=1.54056\text{\AA}$) source equipped with an X'celerator detector. Energy dispersive x-ray spectroscopic data (EDS) was collected using a Noran system S1X (Thermo Electron Corporation, model 6714A01SUS-SN) probe attached to a JEOL JSM-7500F field-emission microscope. $Na_2Ti_3O_7$ was used as a reference to calibrate the EDS for quantitative elemental analysis. Raman spectra were collected with a Spex 1877 0.6m Triple Spectrometer equipped with a Princeton Instruments CCD detector and a Lexel 95 Ar⁺ ion laser operating at 488 nm and 300 mW.

The electrochemical properties of the compounds were evaluated in two-electrode 2032 coin cells containing metallic sodium as the counter electrode. Bulk dry sodium (Sigma Aldrich) was extruded into thin foils and cut to size to make sodium anodes for

these cells. Composite working electrodes were prepared by making a slurry of 70 wt% of the active material, 20-25 wt% acetylene black (Denka, 50% compressed), and 5-10 wt% polyvinylidene difluoride (PVDF) (99.5+%, Aldrich) binder in N-methyl-2-pyrrolidinone (NMP). The active material and the acetylene black were first mixed for 2 hours at 300 rpm in a planetary mill. The slurry was casted on carbon coated aluminum foil (Exopack Advanced Coatings (<http://www.exopackadvancedcoatings.com/2010/02/conductives-current-collector/>)). The electrodes were dried first in air and then under vacuum at 120°C for 12h before being cut to size and weighed. The typical loading and thickness were 5 mg/cm² and 60 μm. The electrolyte used was a solution of 1 M NaPF₆ (Sigma Aldrich) in ethylene carbonate/dimethylene carbonate (EC:DMC; 3:7 mol, from Novolyte Technologies) made in-house and Celgard 3401 separators were used. Galvanostatic cycling experiments at room temperature were carried out with a Bio-logic VMP3 potentiostat/galvanostat.

Results and Discussion

Figure 1a shows a slice of the Na-Ti-O ternary phase diagram, obtained with the phase diagram app at the Materials Project website [26, 27, 28, 29]. The app uses density functional theory to generate compositional phase diagrams at 0K and 0 atm. Phases predicted to be thermodynamically stable are marked with large red dots, and those containing Ti⁴⁺ (i.e., ones that are likely to undergo reversible electrochemical reduction) are located along the bottom of the triangle. Compounds that are very sodium-rich are not likely to be useful in batteries because of their high equivalent weights, but ones lying along the tie line between Na₄TiO₄ and TiO₂ can be considered for this purpose. Na₄TiO₄

itself is an ionic solid with isolated TiO_4 tetrahedra [30] and is therefore probably too insulating to undergo reversible redox intercalation reactions, but $\text{Na}_2\text{Ti}_3\text{O}_7$ and $\text{Na}_2\text{Ti}_6\text{O}_{13}$ both have connected structures suitable for intercalation reactions (Figures 1b and c, [31, 32]). In addition to these three structures, several compounds having the general formulae of $\text{Na}_2\text{Ti}_n\text{O}_{2n+1}$ or $\text{Na}_4\text{Ti}_n\text{O}_{2n+2}$, which lie along the Na_4TiO_4 - TiO_2 tie line, have also been reported in the literature (Table 1, [24, 33, 34, 35, 36, 37, 38, 39]). Many of these are metastable or are more complex than simple ternary compositions (e.g., they are hydrates or are hydroxylated), which is why they do not show up in the calculated phase diagram. Most of these compounds share the general structural features of $\text{Na}_2\text{Ti}_6\text{O}_{13}$ and $\text{Na}_2\text{Ti}_3\text{O}_7$ in that they consist of TiO_6 octahedra connected by edges and corners to form either stepped layered or tunnel structures, with sodium ions located between the layers or within the tunnels. Compositions with low Na/Ti ratios form tunnel structures similar to $\text{Na}_2\text{Ti}_6\text{O}_{13}$, while those with high ratios tend to be stepped layered structures like that exhibited by $\text{Na}_2\text{Ti}_3\text{O}_7$, with the number of TiO_6 octahedra in the steps proportional to n.

The electrochemical behavior of $\text{Na}_2\text{Ti}_6\text{O}_{13}$ in a sodium half-cell configuration is presented in Figure 2. Because all of the titanium in the as-made material is already in the +4 oxidation state, it is not possible to perform electrochemical extraction of sodium from this structure reversibly. Sodium can, however, be inserted at about 0.9V vs. Na^+/Na and subsequently removed. The first cell discharge is complicated by irreversible insertion of sodium into the carbon conductive additive used in the composite electrode and reduction of electrolyte to form a solid electrolyte interface (SEI). Upon subsequent charge, approximately one Na per formula unit can be removed, suggesting that the

intercalation limit is $x=1$ in $\text{Na}_{2+x}\text{Ti}_6\text{O}_{13}$, corresponding to approximately 50 mAh/g. This is close to the discharge capacity observed during subsequent cycles. In the $\text{Na}_2\text{Ti}_6\text{O}_{13}$ structure (Figure 1b), two sodium ions are located in each tunnel, but there are three cubic sites in all. Insertion of an additional sodium ion into the empty site leads to a composition of $\text{Na}_3\text{Ti}_6\text{O}_{13}$ for the fully reduced material, in agreement with the observed behavior. Reversible intercalation of sodium into the $\text{Na}_2\text{Ti}_6\text{O}_{13}$ structure is thus essentially site-limited, and only 1/6 of the available Ti^{4+} is reduced to Ti^{3+} reversibly during cell discharge. In contrast, the capacity for insertion of lithium ions into the $\text{Na}_2\text{Ti}_6\text{O}_{13}$ structure is much higher. Initial discharge capacities of about 150 mAh/g have been reported for $\text{Li}/\text{Na}_2\text{Ti}_6\text{O}_{13}$ cells and up to 250 mAh/g for cells containing the ion-exchanged material, $\text{Li}_2\text{Ti}_6\text{O}_{13}$, with the average potential about 1.5V vs. Li/Li^+ [40]. A recent neutron diffraction study indicated that lithium ions have planar coordination to four oxygen ions in $\text{Li}_2\text{Ti}_6\text{O}_{13}$ whereas sodium ions are located in cubic sites and each one is coordinated to eight oxygens in $\text{Na}_2\text{Ti}_6\text{O}_{13}$ [41]. The different site symmetry and smaller size of the ion means that more lithium can be inserted into $\text{Na}_2\text{Ti}_6\text{O}_{13}$ materials than sodium.

$\text{Na}_2\text{Ti}_3\text{O}_7$, which is more sodium-rich than $\text{Na}_2\text{Ti}_6\text{O}_{13}$, might be expected to have similar site-limitation issues, at first glance. In the as-made material, sodium ions occupy two types of sites, one with nine-fold coordination to oxygens and the second with seven-fold coordination, in the stepped layered structure (Figure 1c). In spite of this, an additional two sodium ions can be inserted to a composition of $\text{Na}_4\text{Ti}_3\text{O}_7$, corresponding to a specific capacity of about 200 mAh/g [42]. The discharge profile in sodium half-cells is flat, characteristic of a two-phase process, and insertion occurs at an unusually low

potential of about 0.3V vs. Na/Na⁺. The exact details concerning the nature of the phase transition upon insertion of sodium have yet to be determined, but the XRD pattern of Na₄Ti₃O₇ bears similarities to that of Na₁₆Ti₁₀O₂₈, a structure in which ten TiO₆ octahedra are linked to form clusters, with sodium ions in either octahedral or prismatic sites between them [43]. The rearrangement of the Na₂Ti₃O₇ structure allows the accommodation of additional sodium ions, but the implications of this for long-term cycling are not yet known. While highly reversible two-phase lithium insertion reactions are known, such as the Li₄Ti₅O₁₂ example given in the Introduction, volume changes are expected to be larger when sodium ions are the intercalants rather than lithium ions. These large changes can result in mismatches and strain that can adversely impact cycle life. These may, however, be ameliorated with careful electrode and cell engineering; for example, a recent optimization study indicates that the electrochemical performance of Na/Na₂Ti₃O₇ cells is dependent on how Na₂Ti₃O₇ is milled with the carbon black conductive additive used in the electrode [44].

As is the case with Na₂Ti₆O₁₃, Na₂Ti₃O₇ can also act as a lithium ion insertion host in lithium half-cell configurations, although the initial capacity is only about 50 mAh/g [45]. This is improved when the material is partially or fully ion-exchanged; e.g., it increases to about 140 mAh/g for Li₂Ti₃O₇. Exchanged variants exhibited flat discharge profiles at about 1.6V vs. Li⁺/Li, again, suggestive of a two-phase mechanism. Upon cycling, the profile evolves into one that is gradually sloping, similar to what is seen in Li/Na₂Ti₃O₇ cells, and XRD patterns on cycled electrodes indicate that the Li₂Ti₃O₇ structure is retained without damage. The electrochemical characteristics strongly suggest that Li insertion processes into this material progress differently than those

associated with sodium. For example, the lithium ions in $\text{Li}_2\text{Ti}_3\text{O}_7$ are thought to occupy tetrahedral sites in the lattice, rather than the 7- and 9-coordinate sites seen in the sodium-containing analog. Lithium ions can then be inserted into two additional vacant tetrahedral sites to give a final composition of $\text{Li}_4\text{Ti}_3\text{O}_7$, close to what is observed.

Of the remaining phases listed in Table 1, several of which can be expected to show electrochemical activity, $\text{Na}_4\text{Ti}_9\text{O}_{20}\cdot n\text{H}_2\text{O}$ is the most easily synthesized. It is readily produced by a hydrothermal method at moderate temperatures of about 200°C . This compound, also known in the literature as “sodium nonatitanate” has been widely used for nuclear waste cleanup, due to its high exchange capacity for Sr^{2+} [46, 47, 48]. The composition varies somewhat with the synthesis conditions and the exact structure remained unknown until recently, although it was assumed to be layered based on the XRD patterns. An intermediate species in the production of TiO_2 nanorods is synthesized hydrothermally under the same conditions as sodium nonatitanate and has an identical XRD pattern. This precursor has now been identified as $\text{NaTi}_3\text{O}_6(\text{OH})\cdot 2\text{H}_2\text{O}$, and the structure solved by automated electron tomography [49]. It is a stacking faulted layered structure consisting of linked $\text{Ti}_6\text{O}_{14}^{4-}$ units with hydroxyl groups located on steps (Figure 3a). In the as-made material, sodium ions are in octahedral sites; these and water molecules occupy interlayer spaces. Upon heating to 600°C , the water is removed irreversibly without affecting the framework [24] but Raman and IR spectroscopic evidence suggest that sodium ions move to different sites and that pinch points between the layers form with bridging Na or H ions between them. Both the hydrated (as-made) form and the anhydrous form are electrochemically active in sodium cells, but only the latter shows good reversibility when cycled. De-intercalation of water, and degradation of

the composite electrode during discharge and charge processes are thought to account for the poor behavior of the hydrated form in sodium cells. The formation of linking bonds in the dehydrated material also serve to stabilize the structure, resulting in the improved cycling that is observed. The discharge profiles of both materials (Figure 4a) are gradually sloping and the average voltage is about 0.5V vs. Na/Na⁺. About 125 mAh/g is obtained for the anhydrous material on the second cycle, with good retention over 20 cycles (Figure 4b). (As with Na/Na₂Ti₆O₁₃ cells, insertion of sodium into the carbon additive and SEI formation contribute to the observed first cycle irreversibility). Details concerning sodium insertion processes into electrodes derived from NaTi₃O₆(OH)•2H₂O are currently lacking, although the removal of water can be expected to free two additional sites per formula unit. These materials are clearly less site-limited than Na₂Ti₆O₁₃, and it is not unreasonable to expect that higher reversible capacities can be obtained once the synthesis and electrode-engineering procedures are optimized.

The low potentials at which sodium insertion processes occur in electrodes based on “sodium nonatitanate”/ NaTi₃O₆(OH)•2H₂O are somewhat reminiscent of the behavior of Na₂Ti₃O₇, although the sloping voltage profiles are indicative of solid solution behavior rather than the two-phase process (flat discharge profile) seen in the latter. X-ray diffraction patterns obtained on partially and fully discharged electrodes are also consistent with a single-phase process throughout the entire composition range; while peak positions and intensities change with the state-of-discharge, no new reflections indicative of a second phase appear. Upon recharge, the XRD pattern of the original phase returns (not shown).

The lithium insertion behavior of $\text{NaTi}_3\text{O}_6(\text{OH})\cdot 2\text{H}_2\text{O}$ -based electrodes differs drastically from that of other ternary titanate phases that have been discussed so far. In the cases of $\text{Li}_4\text{Ti}_5\text{O}_{12}$, $\text{Na}_2\text{Ti}_3\text{O}_7$, and $\text{Na}_2\text{Ti}_6\text{O}_{13}$, lithium insertion occurs at relatively high potentials vs. Li^+/Li (about 1.5-1.6V). In contrast, the behavior of lithium cells containing electrodes based on $\text{NaTi}_3\text{O}_6(\text{OH})\cdot 2\text{H}_2\text{O}$ is similar to that of the sodium cells, exhibiting sloping discharge profiles with an average potential of about 0.5V. The very low potentials at which lithium is inserted into this structure have important implications for lithium ion technologies; if the full theoretical capacity of about 300 mAh/g (corresponding to reduction of all Ti^{4+} to Ti^{3+}) can be cycled, cells utilizing this anode would have higher energy density than those with graphite, due to the greater density of the titanate. At present, reversible capacities of about 120 mAh/g has been demonstrated over 20 cycles for lithium half cells containing electrodes based on $\text{NaTi}_3\text{O}_6(\text{OH})\cdot 2\text{H}_2\text{O}$; in contrast to the case with sodium, and somewhat surprisingly, the as-made material appears to cycle equally as well as the anhydrous form [24].

The results on this phase, although still preliminary, are extremely promising, and warrant its further investigation for use in both lithium ion and sodium ion batteries due to the very low potentials and high capacities. An additional advantage, particularly for dual sodium ion intercalation systems, is the single-phase behavior throughout the entire composition range. Volume changes are expected to occur more gradually during insertion and de-insertion processes in solid solution processes, leading to better cycling behavior than with multi-phase electrodes, where strain can build up at phase boundaries.

Based on the behavior of the layered ternary titanates described above, a structurally related series of titanates can be expected to show good electrochemical

activity towards sodium and lithium insertion processes. These belong to a family of compounds with corrugated layer structures similar to that of the mineral lepidocrocite (FeOOH). The structure of one of these, that of $K_{0.8}[Ti_{1.73}Li_{0.27}]O_4$, made easily by solid state synthesis, is depicted in Figure 3b. Titanates with lepidocrocite structures are not simple ternary compositions but have the general formula $A_x[Ti_{2-y}M_y]O_4 \cdot zH_2O$, where A is K, Rb, or Cs and M is Mg, Co, Ni, Cu, Zn, Mn, Fe, Li, or a vacancy [50]. M cations are located in the transition metal layers and A cations between the layers. The value of x is generally between 0.6-0.8 when A is Rb or Cs, and 0.7-0.9 when A is K and M is Mg, Zn, Ni, Cu, Fe, or Mn [51]. Lepidocrocite structures with more than one type of alkali metal ion on the A sites (e.g., K+Rb, K+Li) can also be synthesized [52]. While the direct synthesis of titanate lepidocrocite structures with A=Na has not been reported, these variants can be readily prepared via ion exchange of the K, Rb, or Cs-containing forms [53].

As with “sodium nonatitanate”, the properties of many of the lepidocrocite titanates make these compounds interesting for ion exchange and other applications [54] and imply that they may undergo electrochemical intercalation reactions readily. The compositional variability of these compounds also means that the electrodes can be custom-tailored for the desired electrochemical properties. For battery applications, compositions should be chosen that minimize the equivalent weight so that the maximum specific theoretical capacity can be achieved. Thus, for example, M should be a lightweight element and the value of y should be kept as small as possible to maximize the amount of electroactive Ti^{4+} in the as-made material (alternatively, M can be an electroactive metal such as Mn). To avoid problems with site limitations, the value of x

should also be as low as feasible. During ion exchange processes, changes in site symmetries and occupancies can occur that may ameliorate this issue, particularly if a small ion is exchanged for a larger one. Because Ti is always tetravalent in these structures, the values of x and y in the $A_x[Ti_{2-y}M_y]O_4 \cdot zH_2O$ formula are correlated and depend on the redox state of M. Thus, $y=x/4$ for a vacancy, $x/3$ for M^+ , $y=x/2$ for M^{2+} , and $y=x$ for M^{3+} so that reducing x also results in reducing y. Using these principles, it is possible to design electrodes with theoretical specific capacities in excess of 200 mAh/g.

For studies in sodium half-cells, $K_{0.8}[Ti_{1.73}Li_{0.27}]O_4$ (KTL) was synthesized by a solid state procedure and subjected to acid-leaching to produce the protonated form (H-KTL). The sodium form (Na-H-KTL) was then produced by ion-exchanging H-KTL. The EDS data in figure 5a show that the acid leaching completely removed the potassium ions from KTL and that ion exchange resulted in the production of a sodium-containing phase. In addition, the absence of the high frequency Raman peak [55] in the protonated form and reappearance of this peak in the sodium form are consistent with complete removal of K and insertion of Na ions into the interlayer galleries (Figure 5b) during these procedures. The interlayer distance, calculated from the XRD patterns in figure 5c, increases from 7.68Å in the K-titanate (space group: Cmc₂m) to 9.05Å in the protonated form (space group: Immm) and to 11.47Å in the sodium form (space group: Immm). The changes in interlayer spacings and overall symmetries are consistent with differences in the arrangements of cations and the amount of water in the galleries [25], but the basic structural feature of corrugated layers is maintained for all three materials.

The sodium half cell discharge profiles of (KTL), (H-KTL) and (Na-H-KTL) are shown in Figure 6. Based on reduction of all of the Ti^{4+} to Ti^{3+} , the theoretical capacity of

the K-titanate is 257 mAh/g, but much less than this is obtained during the first discharge. Although not all of the A sites are occupied, the large size of the potassium ions means they are only 1.5 Å apart, which limits the insertion capability. Much higher initial capacities are obtained for the ion-exchanged version, which is less site-limited. The discharge profiles of both materials are gradually sloping like those of the electrodes based on $\text{NaTi}_3\text{O}_6(\text{OH})\cdot 2\text{H}_2\text{O}$, but with a somewhat higher average potential, and the lithium insertion processes mirror that of the sodium ones. As with the $\text{NaTi}_3\text{O}_6(\text{OH})\cdot 2\text{H}_2\text{O}$ -based electrodes, the cycling characteristics of the dehydrated electrode are superior to the hydrated version. The capacity retention of the lepidocrocite Na-titanate in sodium half-cells is a function of the voltage limits that are used and the composite electrode composition. Better results are obtained when the lower voltage limit during discharge is raised (Figure 7) or when a more compliant polyacrylic acid (PAA) binder is used instead of the conventional polyvinylidene fluoride (PVdF). These results suggest that volume changes upon intercalation of sodium are large enough to result in degradation of this material during deep discharge or when a stiff binder that cannot maintain the integrity of the electrode is used. Lepidocrocite titanate host structures with low charge densities, defined as $x/2ac$, where a and c are unit cell parameters and x refers to the formula $\text{A}_x[\text{Ti}_{2-y}\text{M}_y]\text{O}_4$, are known to intercalate bulky guest species such as solvents and solvated cations readily. This phenomenon can result in exfoliation and has been exploited in the past to prepare colloidal suspensions of nanosheets [56, 57]. Thus, increasing the charge density by adjusting the lepidocrocite composition can probably be used to improve the reversibility of the electrode if exfoliation cannot be prevented by other means.

It is clear from these examples that titanates manifest a remarkable variability in their electrochemical characteristics. Both solid solution and multi-phase behavior during intercalation processes has been observed, and insertion of alkali metal cations occurs at widely differing potentials, depending on host structure, the phase behavior, and the nature of the intercalant. Although sodium reduction occurs only about 0.3V higher than lithium reduction vs. the standard hydrogen electrode (S.H.E.), potential differences between the insertion processes of sodium and lithium into the titanates vary as much as 1V (Figure 8) and sodium insertion processes frequently occur at lower absolute potentials than lithium, due to differences in site symmetries. The very low potentials at which sodium insertion processes take place in some of the titanate anodes suggest that higher theoretical energy densities for sodium ion batteries could be obtained in optimized systems than in the analogous Li ion devices utilizing the $\text{Li}_4\text{Ti}_5\text{O}_{12}$ anode. Moreover, the very low potentials at which lithium insertion occurs in some of the layered titanates (those based on $\text{NaTi}_3\text{O}_6(\text{OH})\cdot 2\text{H}_2\text{O}$ and lepidocrocite structures) should also allow higher energy Li ion batteries with titanate anodes to be developed.

Conclusions

The electrochemical characteristics of several sodium titanate host structures have been presented in this paper. While the emphasis herein is primarily on the development of anode materials for sodium ion batteries, it is instructive to compare the behaviors of these materials in sodium and lithium half-cells. For example, the tunnel compound $\text{Na}_2\text{Ti}_6\text{O}_{13}$ has low capacity for sodium insertion, but much higher capacity for lithium due to differing site symmetries for the two intercalants. The most promising materials for sodium systems appear to be layered materials based on $\text{Na}_2\text{Ti}_3\text{O}_7$,

$\text{NaTi}_3\text{O}_6(\text{OH})\cdot 2\text{H}_2\text{O}$, and lepidocrocite structures because they are less site-limited than the tunnel compounds and insert sodium at very low potentials. The latter two categories of materials also demonstrate good reversibility in preliminary cycling tests. Another attractive feature of the lepidocrocite-type materials is the possibility of varying the composition to maximize capacities, although care may need to be taken to tune the charge density to prevent losses due to exfoliation. Lithium insertion processes into the titanate hosts differ substantially from the sodium insertion processes, often occurring at very different absolute potentials. An intriguing characteristic of the $\text{NaTi}_3\text{O}_6(\text{OH})\cdot 2\text{H}_2\text{O}$ and lepidocrocite-based materials is that they also insert lithium at much lower potentials than other known titanates. The low potentials at which lithium and sodium insert into these materials have important implications for the development of high energy density dual intercalation devices, whether based on lithium or sodium.

Acknowledgment

This work was supported by the Laboratory Directed Research and Development Program of Lawrence Berkeley National Laboratory under U.S. Department of Energy Contract DE-AC02-05CH11231.

References

-
1. <http://www.marketresearch.com/David-Company-v3832/Lithium-Ion-Batteries-Outlook-Alternative-6842261/>
 2. Research Center for Energy Economics (<http://www.ffe.de/en/>)

-
3. Z. Yang, J. Zhang, M. C. W. Kintner-Meyer, X. Lu, D. Choi, J. P. Lemmon, J. Liu, *Chem. Rev.* 111, 3577 (2011)
 4. V. Palomares, P. Serras, I. Villaluenga, K. B. Hueso, J. Carretero-González, T. Rojo, *Energy & Environ. Sci.* 5, 5884 (2012)
 5. M. D. Slater, D. Kim, E. Lee, M. M. Doeff, C.S. Johnson, *Adv. Funct. Mater.* 23, 947 (2013)
 6. M. M. Doeff, M. Y. Peng, Y. Ma, L.C. De Jonghe, *J. Electrochem. Soc.* 141, L145 (1994)
 7. J. F. Whitacre, A. Tevar, S. Sharma, *Electrochem. Commun.* 12, 463 (2010)
 8. H. Kim, D. J. Kim, D.-H. Seo, M. S. Yeom, K. Kang, D. K. Kim, Y. Jung, *Chem. Mater.* 24, 1205 (2012)
 9. D. Kim, S.-H. Kang, M. Slater, S. Rood, J. T. Vaughey, N. Karan, M. Balasubramanian, C. S. Johnson, *Adv. Energy Mater.* 1, 333 (2011)
 10. M. Sathiya, K. Hemalatha, K. Ramesha, J.-M. Tarascon, A. S. Prakash, *Chem. Mater.* 24, 1846 (2012)
 11. B. L. Ellis, W. R. M. Makahnouk, Y. Makimura, K. Toghill, L. F. Nazar, *Nat. Mater.* 6, 749 (2007)
 12. M. M. Doeff, Y. Ma, S. J. Visco, L.C. De Jonghe, *J. Electrochem. Soc.* 140, L169 (1993)
 13. D. A. Stevens, J. R. Dahn, *J. Electrochem. Soc.* 147, 1271 (2000)
 14. S. Komaba, W. Murata, T. Ishikawa, N. Yabuuchi, T. Ozeki, T. Nakayama, A. Ogata, K. Gotoh, K. Fujiwara, *Adv. Funct. Mater.* 21, 3859 (2011)

-
15. X. Xia, M. N. Obrovac, J. R. Dahn, *Electrochem. and Sol. State Lett.* 14, A130 (2011)
 16. V. L. Chevrier, G. Ceder, *J. Electrochem. Soc.* 158, A1011 (2011)
 17. J. Cabana, L. Monconduit, D. Larcher, M. R. Palacin, *Adv. Mater.* 22, E170 (2010)
 18. Z. Yang, D. Choi, S. Kerisit, K. M. Rosso, D. Wang, J. Zhang, G. Graff, J. Liu, J. Power Sources 192, 588 (2009).
 19. K. C. Kam, M. M. Doeff, *Mater. Matters* 7, 56 (2012)
 20. R. D. Shannon, *Acta Cryst. A* 32, 751 (1976)
 21. H. Xiong, M. D. Slater, M. Balasubramanian, C. S. Johnson, T. Rajh, *J. Phys. Chem. Lett.* 2, 2560 (2011)
 22. L. Zhao, H.-L. Pan, Y.-S. Hu, H. Li, L.-Q. Chen, *Chin Phys. B* 21, 028201 (2012)
 23. Y. Sun, L. Zhao, H. Pan, X. Lu, L. Gu, Y.-S. Hu, H. Li, M. Armand, Y. Ikuhara, L. Chen, X. Huang, *Nature Commun.* DOI: 10.1038/ncomms2878
 24. M. Shirpour, J. Cabana, M. Doeff, *Energy & Environ. Sci.*, (2013)
DOI:10.1039/C3EE41037D
 25. T. Sasaki, F. Kooli, M. Iida, Y. Michius, S. Takenouchi, Y. Yajima, F. Izumi, B. C. Chakoumakos, M. Watanabe, *Chem. Mater.* 10, 4123 (1998)
 26. A. Jain, G. Hautier, C. Moore, S.P. Ong, C. Fischer, T. Mueller, K. Persson, G. Ceder, *Comp. Mater. Sci.* 50, 2295 (2011)
 27. S. P. Ong, A. Jain, G. Hautier, M. Kocher, S. Cholia, D. Gunter, D. Bailey, D. Skinner, K. Persson, G. Ceder, The Materials Project, <http://materialsproject.org/>
 28. S.P. Ong, L. Wang, B. Kang, G. Ceder, *Chem. Mater.* 20, 1798 (2008)

-
29. A. Jain, G. Hautier, S.P. Ong, C. Moore, C. Fischer, K. Persson, G. Ceder, *Phys Rev B* 84, 045115 (2011)
 30. R. Olazcuaga, J.-M. Reau, M. Devalette, G. Le Flem, P. Hagenmuller, *J. Sol. State Chem.* 13, 275 (1975)
 31. S. Andersson, A.D. Wadsley, *Acta Cryst.* 14, 1245 (1961)
 32. S. Andersson, A.D. Wadsley, *Acta Cryst.* 15, 194 (1962)
 33. M. Dion, Y. Piffard, M. Tournoux, *J. Inorg. Nucl. Chem.* 40, 917 (1978)
 34. V.B. Nalbandyan, *Russ. J. Inorg. Chem.* 45, 757 (2000)
 35. M. Avdeev, A. Kholkin, *Acta Cryst. C* 56, e539 (2000)
 36. V. B. Nalbandyan, M. Yu. Avdeev, V. V. Lukov, *Russ. J. Inorg. Chem.* 43, 148 (1998)
 37. A.D. Wadsley and W. G. Mumme, *Acta Cryst.* B24, 392 (1968)
 38. Y. Bando, *Acta Cryst.* A38, 211 (1982)
 39. Y. Bando, M. Watanabe, Y. Sekikawa, *J. Sol. State Chem.* 33, 413 (1980)
 40. J. C. Pérez-Flores, A. Kuhner, F. García-Alvarado, *J. Power Sources* 196, 1378 (2011)
 41. K. Kataoka, J. Awaka, N. Kijima, H. Hayakawa, K.-I. Ohshima, J. Akimoto, *Chem. Mater.* 23, 2344 (2011)
 42. P. Senguttuvan, G. Rousse, V. Seznec, J.-M. Tarascon, M. R. Palacín, *Chem. Mater.* 23, 4109 (2011)
 43. G. Ilyushin, *Crystallogr. Reports* 51, 715 (2006)
 44. A. Rudola, K. Saravanan, C. W. Mason, P. Balaya, *J. Mater. Chem. A* 1, 2653 (2013)

-
45. K. Chiba, N. Kijima, Y. Takahashi, Y. Idemoto, J. Akimoto, *Solid State Ionics* 178, 1725 (2008)
 46. J. Lehto, A. Clearfield, *J. Radioanal. Nucl. Chem. Lett.* 118, 1 (1987)
 47. A. Clearfield, J. Lehto, *J. Sol.State Chem.*, 73, 98 (1988)
 48. A. Merceille, E. Weinzapfel, Y. Barré, A. Grandjean, *Adsorption* 17, 967 (2011)
 49. I. Andrusenko, E. Magnaioli, T. E. Gorelik, D. Koll, M. Panthöfer, W. Tremel, U. Kolb, *Acta Cryst. B*67, 218 (2011)
 50. A. F. Reid, W.G. Mumme, A. D. Wadsley, *Acta Cryst. B*24, 1228 (1968)
 51. D. Groult, C. Mercey, B. Raveau, *J. Solid State Chem.* 32, 289 (1973)
 52. R.S. Roth, H.S. Parker, W. S. Brower, *Mater. Res. Bull.* 8, 327 (1973)
 53. W.A. England, J.E. Birkett, J. P. Goodenough, and P.J. Wiseman, *J. Solid State Chem.* 49, 300 (1983)
 54. Y. Matsumoto, A. Funatsu, D. Matsuo, U. Unal, *J. Phys. Chem. B* 105, 10893 (2001)
 55. T. Beuvier, M. Richard-Plouet, L. Brohan, *J. Phys. Chem. C* 114, 7660 (2010)
 56. T. Sasaki, M. Watanabe, *J. Am. Chem. Soc.* 120, 4682 (1998)
 57. T. Sasaki, M. Watanabe, H. Hashizume, H. Yamada, H. Nakazawa, *J. Am. Chem. Soc.* 118, 8329 (1996)

Table 1. Sodium titanates, $\text{Na}_2\text{Ti}_n\text{O}_{2n+1}$ or $\text{Na}_4\text{Ti}_n\text{O}_{2n+2}$, reported in the literature.

Compound	Preparation	Reference	Structure
$\text{Na}_2\text{Ti}_3\text{O}_7$	$\text{Na}_2\text{CO}_3 + \text{TiO}_2$, 1000°C	[31]	stepped layered, $m=3^a$
$\text{Na}_2\text{Ti}_4\text{O}_9$	Ion exchange of $\text{Ti}_2\text{Ti}_4\text{O}_9$	[33]	stepped layered, $m=4^a$
$\text{Na}_4\text{Ti}_5\text{O}_{12}$, LT	Na_2CO_3 , NaNO_3 , TiO_2 , 690°C	[34, 35]	Distorted close- packed
$\text{Na}_4\text{Ti}_5\text{O}_{12}$, HT	Air oxidation of $\text{Na}_{4+x}\text{Ti}_5\text{O}_{12}$	[36]	complex layered
$\text{Na}_2\text{Ti}_6\text{O}_{13}$	$\text{Na}_2\text{CO}_3 + \text{TiO}_2$, 800-1000°C	[32]	tunnel
$\text{Na}_2\text{Ti}_7\text{O}_{15}$	$\text{Na}_2\text{C}_2\text{O}_4$, TiO_2 , Al_2O_3 , 1300°C	[37]	tunnel
$\text{Na}_2\text{Ti}_9\text{O}_{19}$	$\text{NaOH} + \text{TiO}_2$, hydrothermal, 550°C	[38, 39]	tunnel
$\text{Na}_4\text{Ti}_9\text{O}_{20} \cdot n\text{H}_2\text{O}$ $=\text{NaTi}_3\text{O}_6(\text{OH}) \cdot 2\text{H}_2\text{O}$	$\text{NaOH} + \text{Ti}(\text{iPrOH})_4^b$ hydrothermal, 200°C	[24]	stepped layered, $m=6^a$

a. m refers to the number of TiO_6 octahedra per step.

b. $\text{Ti}(\text{iPrOH})$ =titanium isopropoxide

Figure Captions

Figure 1. (a) Section of the Na-Ti-O compositional phase diagram, generated using the Materials Project website phase diagram app (see text). Compositions predicted to be thermodynamically stable at 0K and 0 atm are marked with large red dots. Compositions located along the tieline between Na_4TiO_4 and TiO_2 , marked with a double arrow, are of interest for battery applications. **(b)** Structure of $\text{Na}_2\text{Ti}_6\text{O}_{13}$, in which TiO_6 octahedra (in gold) are joined by corners and edges to form a tunnel structure, into which sodium ions (pink spheres) are located. **(c)** Structure of $\text{Na}_2\text{Ti}_3\text{O}_7$, in which TiO_6 octahedra (in blue) are joined by corners and edges to form a stepped layered structure, with sodium ions (cyan spheres) located between the layers.

Figure 2. First cycle of a Na/ $\text{NaTi}_6\text{O}_{13}$ cell, discharged and charged at 0.01 mA/cm^2 . Inset shows the specific capacity as a function of cycle number.

Figure 3. (a) Structure of “sodium nonatitanate”, recently shown to be identical to that of $\text{NaTi}_3\text{O}_6(\text{OH})\cdot 2\text{H}_2\text{O}$. TiO_6 octahedra (in light blue) link to form $\text{Ti}_6\text{O}_{14}^{4-}$ units, which form layers between which sodium ions (yellow spheres) and water molecules (oxygens of H_2O depicted as dark blue spheres) are located. OH groups are located at the steps. **(b)** Structure of $\text{K}_{0.8}[\text{Ti}_{1.73}\text{Li}_{0.27}]\text{O}_4$ with the lepidocrocite structure. TiO_6 and LiO_6 octahedra (in pink) share edges to form zigzag layers, between which potassium ions (gray spheres) are located.

Figure 4. (a) Voltage profile and **(b)** specific discharge capacity versus cycle number for the hydrous and the dehydrated nonatitanate in Na half-cells cycled between 1.5 and 0.1 V at 0.15 mA/cm^2 (30 mA/g). Figures adapted from reference [24].

Figure 5. (a) EDS data (b) Raman spectra, and (c) XRD patterns of the lepidocrocite K-titanate (KTL), the protonated form (H-KTL), and the sodium form (Na-H-KTL). The SEM stubs used to mount the samples give rise to the weak Al and C peaks seen in the EDS data, and Cl⁻ is from HCl used to leach the H-KTL sample. An arrow and dashed line mark the position of a high frequency Raman peak diagnostic of the presence or absence of alkali metal cations in the interlayer spaces.

Figure 6. Voltage versus specific capacity for the lepidocrocite K-titanate (KTL), the protonated form (H-KTL), and the sodium form (Na-H-KTL) in Na half-cells cycled between 2 and 0.1 V at 0.20 mA/cm² (40 mA/g).

Figure 7. Specific discharge capacity as a function of cycle number for the sodium form of lepidocrocite titanate (Na-H-KTL) in Na half-cells discharged to different voltage limits, cycled at 0.20 mA/cm² (40 mA/g).

Figure 8. Sodium and lithium insertion potentials of titanates discussed in this paper, plotted vs. the standard hydrogen electrode (S. H. E.). Average potentials are marked with blue open squares (lithium) or red filled circles (sodium) and lines mark the potential range over which insertion occurs for electrodes exhibiting solid solution behavior. NNT= “sodium nonatitanate” and refers to electrodes based on NaTi₃O₆(OH)•2H₂O.

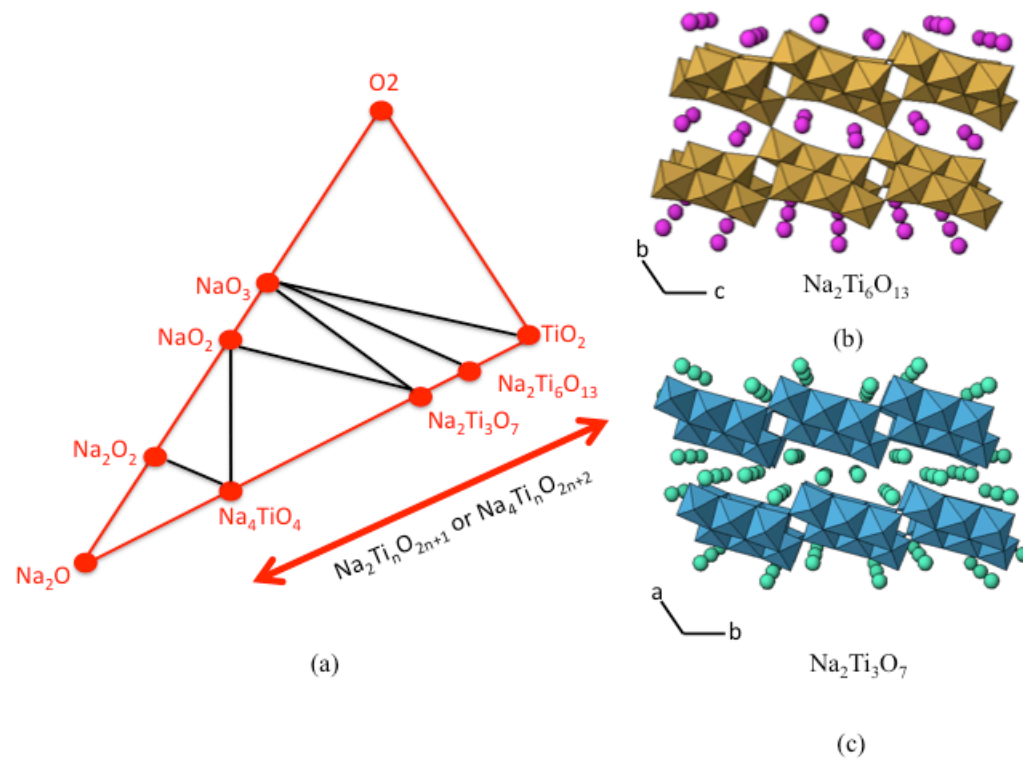


Figure 1

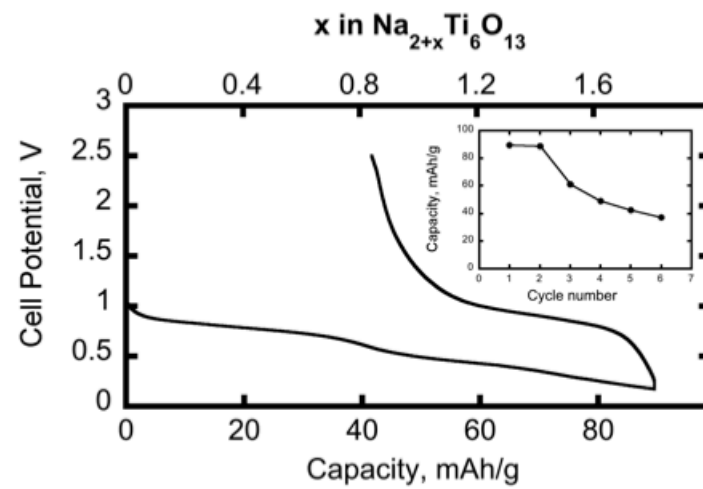


Figure 2

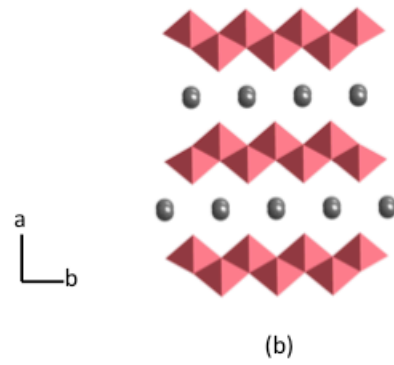
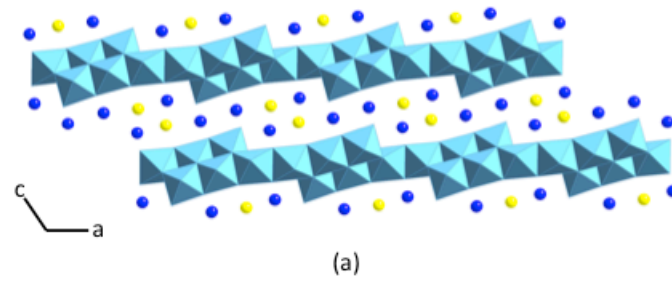
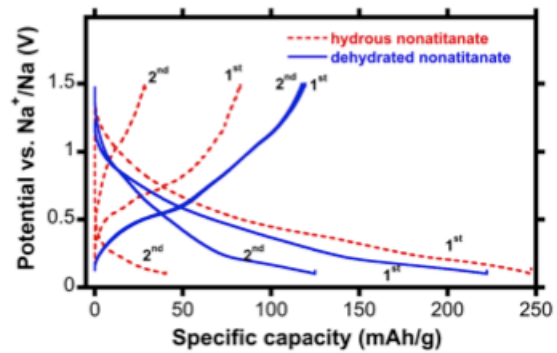
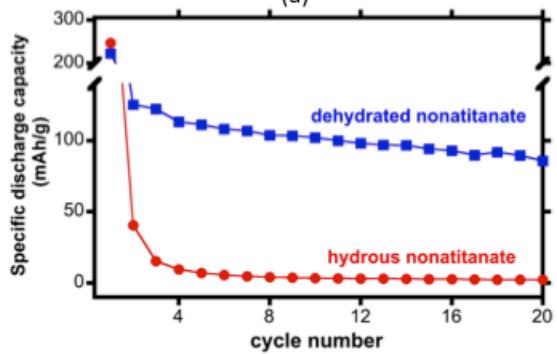


Figure 3



(a)



(b)

Figure 4

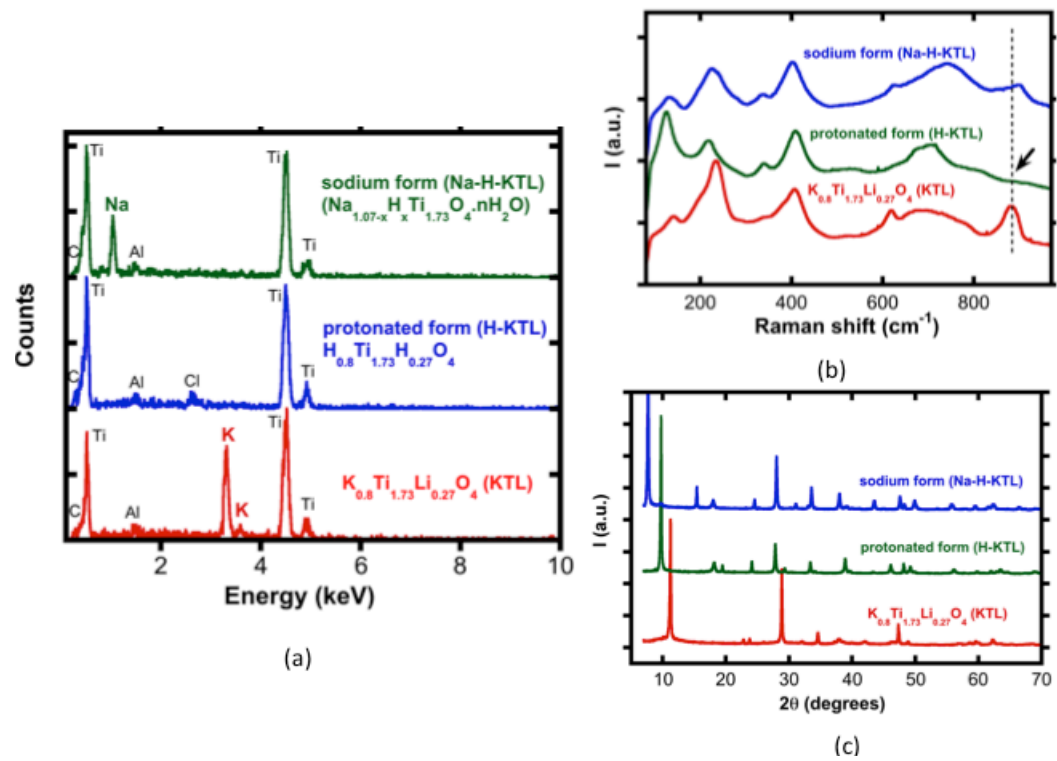


Figure 6

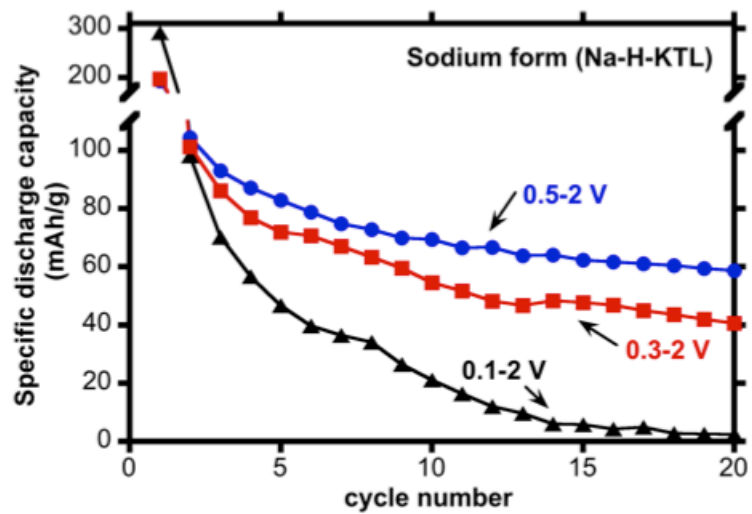


Figure 7

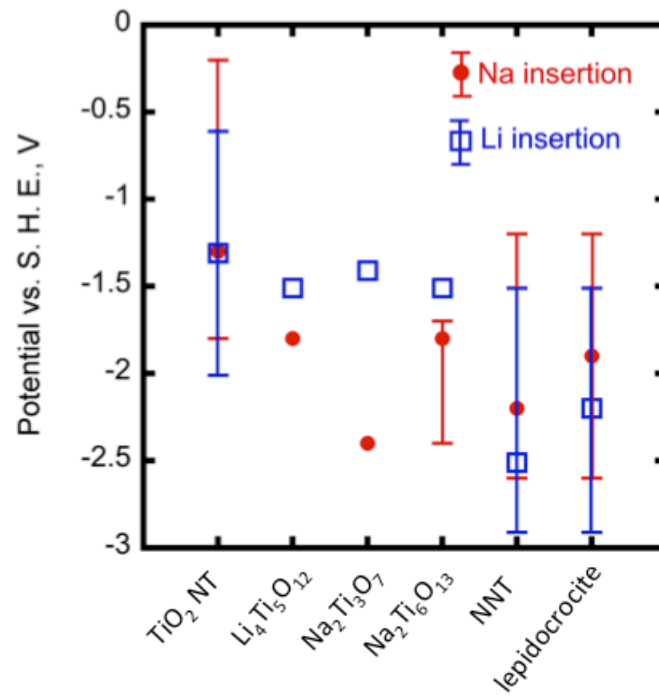


Figure 8